arXiv:1603.05718v1 [math.NA] 17 Mar 2016

Lagrangian Particle Method for Compressible Fluid Dynamics

Hsin-Chiang Chen[a], Roman Samulyak[1a,b], Wei Li[a]

[a] *Department of Applied Mathematics and Statistics, Stony Brook University, Stony Brook, NY 11794*
[b] *Computational Science Center, Brookhaven National Laboratory, Upton, NY 11973*

Abstract

A new Lagrangian particle method for solving Euler equations for compressible inviscid fluid or gas flows is proposed. Similar to smoothed particle hydrodynamics (SPH), the method represents fluid cells with Lagrangian particles and is suitable for the simulation of complex free surface / multiphase flows. The main contributions of our method, which is different from SPH in all other aspects, are (a) significant improvement of approximation of differential operators based on a polynomial fit via weighted least squares approximation and the convergence of prescribed order, (b) an upwinding second-order particle-based algorithm with limiter, providing accuracy and long term stability, (c) elimination of the dependence on artificial parameters such as the smoothening length in SPH, causing difficulties in the case of large density changes, and (d) accurate resolution of states at free interfaces. Numerical verification test demonstrating the convergence order are presented as well as examples of complex free surface flows.

Keywords: Lagrangian fluid mechanics, particle method, generalized finite differences
2000 MSC: 65M06, 70F99, 76T10

1. Introduction and Motivation

High resolution Lagrangian methods are essential for achieving predictive simulations of a wide spectrum of complex free surface / multiphase

[1]Corresponding author, roman.samulyak@stonybrook.edu

problems. Most widely used approaches for the simulation of multiphase problems are based on Eulerian meshes enhanced with special algorithms for resolving interfaces such as the volume-of-fluid [3], the level set method [4], arbitrary Lagrangian - Eulerian methods [5], or the method of front tracking [6] which is a hybrid method involving a moving Lagrangian mesh over a fixed Eulerian mesh. In addition, they often use various adaptive features such as adaptive mesh refinement. These and finite element methods, most common for engineering problems with irregular geometries, require complex computationally intensive methods for the generation of high quality meshes.

Theoretically, the traditional Lagrangian formulation of fluid dynamics [2] is the basis for the most natural and accurate method for the simulation of complex free surface and multiphase systems, but it suffers from the mesh distortion problem in unsteady, turbulent flows. As a result, the Lagrangian methods are widely used only in 1D for all problems except the dynamics of solids that is characterized by small deformations. The overwhelming majority of solid dynamics codes use finite element-based Lagrangian methods, the fact that speaks for advantages of Lagrangian approaches within their applicability range.

A way to extend the Lagrangian method to 3D was proposed in smooth particle hydrodynamics (SPH). SPH [7, 8] is a Lagrangian particle method in computational fluid dynamics in which deforming Lagrangian cells are replaced with particles. SPH eliminates the main mesh tangling difficulty of the original Lagrangian method while retaining many of its advantages. Due to its Lagrangian nature, SPH is strictly mass-conservative and capable of robustly handling interfaces of arbitrary complexity in the simulation of free surface and multiphase flows. The representation of matter by particles provides adaptivity to density changes. Not only does this improve the traditional adaptive mesh refinement of structural meshes, that introduces sharp boundaries between mesh patches of different resolution, but also it enables simulations of large ranges of spatial scales (for instance expansion into vacuum and matter islands separated by large vacuum domains).

However the major drawback of SPH is a very poor accuracy of discrete differential operators. It is widely accepted [10, 11], including original SPH developers [8], that the traditional SPH discretization has zero-order convergence for widely used kernels. The SPH discretization of derivatives is convergent to the order consistent with the interpolating polynomial for the kernel function only if particles are located on a rectangular mesh (which is not the case for unsteady flows). In addition, it depends on artificial pa-

rameters, in particular on the smoothening radius, causing major difficulties in the case of large density changes. The reason why SPH produces stable and reasonable results for certain problems, despite using inaccurate and non-convergent discretization of differential operators, is its connection to the Lagrangian / Hamiltonian dynamics of particles [13]. In particular, the traditional discrete SPH equations for the compressible Euler equations are not accurate, but they accurately represent equations of the Lagrangian dynamics of particles interacting via isentropic potentials. The Lagrangian and Hamiltonian properties are also responsible for the long term stability of the traditional SPH. But the Hamiltonian dynamics of particles only approximately represent the dynamics of continuum hydrodynamic systems, and the isentropic interaction energy places additional restrictions.

A number of 'modern' or 'corrected' SPH methods have been developed in recent years (see [10] and reviews [8, 11]). They include the moving-least-squares SPH, 'Godunov'-SPH, P-SPH, PHANTOM etc. But they all improve certain features of SPH at the expense of other properties such as conservation, long-time stability, or prohibitively large number of neighbors that causes other problems. They all still have zero-convergence order, except for the 1st order convergent, moving-least-squates SPH [10], that suffers from long-time stability and other issues. A new class of convergent, mesh-free hydrodynamic simulation methods was developed in [11].

We have proposed a new Lagrangian particle method for solving compressible Euler equations that eliminates major deficiencies of SPH: the dependence on a parameter called smoothening length, the presence of large linear errors in SPH differential operators, and ensures long term stability via upwinding discretization methods. Significantly different from SPH in most of approximations, our method is also easily generalizable to coupled system of hyperbolic and elliptic or parabolic PDE's for other physics processes.

In the Lagrangian particle method, approximations of spatial derivatives are obtained by employing a local polynomial fit known also as the generalized finite difference (GFD) method [16]. The main idea is to find closest neighbors of each particle and approximate the spatial derivative of a certain physical quantity the particle location as a linear combination of this quantity at neighboring particles. The optimal coefficients in this linear combination are calculated by solving a least squares problem. Second order accurate spatial discretization is used in the current algorithm, but the GFD method makes it possible to use higher order discretizations with increased particle neighborhoods. Our algorithms uses much smaller number of neighbor parti-

cles compared to the Godunov-SPH or other recent SPH modifications that may require hundreds of particles [11]. An application example of the GFD method to the advection-diffusion equation is given in [12].

The conservative Lagrangian formulation of Euler equations is transformed into a quasi-linear form, and an upwinding scheme is employed for the numerical integration. Multiple spatial dimensions are resolved using a Strang splitting method for Euler equations. Research on algorithms for elliptic problems involving geometrically complex boundaries and interfaces is in progress. Together with hyperbolic solvers, they form the basis for simulations of complex multiphysics and multiphase systems. The Lagrangian particle method has been implemented in all dimensions, but algorithms for a parallel code for solving three-dimensional Euler equations will be reported in a forthcoming paper. The main goal of the present work is to introduce main ideas of the Lagrangian particles dynamics and to present verification tests.

The paper is organized as follows. Section 2 contains the main governing equations. Numerical discretization and main algorithms of the Lagrangian particle dynamics are presented in Section 3. Section 4 presents verification tests and accuracy studies. We conclude this work by a summary of our results and perspectives for the future work.

2. Governing Equations

Consider the one-dimensional Lagrangian formulation of the Euler equations, written in the conservative form [1, 2]

$$U_t^{'} + \left[F(U^{'})\right]_x = 0, \tag{1}$$

$$U^{'} = \begin{pmatrix} V \\ u \\ E \end{pmatrix}, \; F(U^{'}) = V_0 \begin{pmatrix} -u \\ P \\ Pu \end{pmatrix}, \tag{2}$$

where V is the specific volume, u is the velocity, E is the specific total energy, and P is the pressure.

Let's assume that the equation of state (EOS) is in the form $e = f\,(P, V)$, where e is the specific internal energy, $e = E - u^2/2$. Equations (1) and (2) can be written using $U = [V \; u \; P]^T$ as the state vector as follows

$$U_t + A(U)U_x = 0, \tag{3}$$

$$U = \begin{pmatrix} V \\ u \\ P \end{pmatrix}, \quad A(U) = V_0 \begin{pmatrix} 0 & -1 & 0 \\ 0 & 0 & 1 \\ 0 & K & 0 \end{pmatrix}, \tag{4}$$

where

$$K = \left(P + \frac{\partial e}{\partial V} \right) \Big/ \frac{\partial e}{\partial P} \, . \tag{5}$$

For example, using the polytropic gas EOS

$$e = \frac{PV}{\gamma - 1}, \tag{6}$$

where γ is the ratio of specific heats, we obtain

$$A(U) = V_0 \begin{pmatrix} 0 & -1 & 0 \\ 0 & 0 & 1 \\ 0 & (\frac{c}{V})^2 & 0 \end{pmatrix}, \tag{7}$$

where $c = \sqrt{\gamma PV}$ is the speed of sound. Note that the transformation is exact (i.e. not a result of linerization). If the matrix A is diagonalized as $A = R\Lambda R^{-1}$, equations (3) and (4) become

$$U_t + R\Lambda R^{-1} U_x = 0,$$

$$R^{-1} U_t + \Lambda R^{-1} U_x = 0, \tag{8}$$

where

$$R^{-1} = \begin{pmatrix} 1 & 0 & \frac{1}{K} \\ 0 & -\frac{1}{2\sqrt{K}} & -\frac{1}{2K} \\ 0 & \frac{1}{2\sqrt{K}} & -\frac{1}{2K} \end{pmatrix}, \quad R = \begin{pmatrix} 1 & 1 & 1 \\ 0 & -\sqrt{K} & \sqrt{K} \\ 0 & -K & -K \end{pmatrix},$$

$$\Lambda = V_0 \begin{pmatrix} 0 & & \\ & \sqrt{K} & \\ & & -\sqrt{K} \end{pmatrix} \tag{9}$$

Based on the governing equations (8) and (9), we have developed stable, particle-based, upwinding numerical schemes for the system of Euler's equations. Details are described in the next section.

3. Numerical Discretization and Main Algorithms

3.1. Discrete Lagrangian Equtions

To solve numerically the hyperbolic system of PDE's (8) and (9), the medium (compressible fluid or gas) is discretized by a distribution of particles. Each particle represents a Lagrangian fluid cell of equal mass, and stores states of the continuum medium such as density (that is proportional to the number density of Lagrangian particles), pressure, internal energy, velocity, as well as material properties and pointers to data structures containing material models, such as the EOS.

To construct a Lagrangian upwinding scheme, we represent the system (8)-(9) in the following component-wise form

$$\begin{aligned} V_t + \frac{1}{K} P_t &= 0, && (10)\\ -\frac{1}{2\sqrt{K}} u_t - \frac{1}{2K} P_t &= -V_0\sqrt{K}\left[-\frac{1}{2\sqrt{K}} u_x - \frac{1}{2K} P_x\right], && (11)\\ \frac{1}{2\sqrt{K}} u_t - \frac{1}{2K} P_t &= V_0\sqrt{K}\left[\frac{1}{2\sqrt{K}} u_x - \frac{1}{2K} P_x\right]. && (12) \end{aligned}$$

As $K > 0$ for a thermodynamically consistent EOS, equation (11) describes waves propagating from left to right, and equation (12) describes waves propagating from right to left. For an upwinding scheme, the spatial derivatives u_x and P_x will be computed on stencils within the corresponding physical domains of dependence. Adding the subscripts l and r to the spatial derivatives in equations (11) and (12), respectively, to indicate that these terms, in the discrete form, will be computed using one-sided derivatives, and solving for the temporal derivatives, we obtain

$$\begin{aligned} V_t &= \frac{V_0}{2}\left(u_{xr} + u_{xl}\right) - \frac{V_0}{2\sqrt{K}}\left(P_{xr} - P_{xl}\right), && (13)\\ u_t &= \frac{V_0\sqrt{K}}{2}\left(u_{xr} - u_{xl}\right) - \frac{V_0}{2}\left(P_{xr} + P_{xl}\right), && (14)\\ P_t &= -\frac{V_0 K}{2}\left(u_{xr} + u_{xl}\right) + \frac{V_0\sqrt{K}}{2}\left(P_{xr} - P_{xl}\right). && (15) \end{aligned}$$

An important component of a particle-based numerical scheme is the calculation of differential operators based on states at the location of particles.

In Section 3.3, we describe in detail a method for both numerical differentiation and interpolation based on local polynomial fitting. In this section, we simply assume that we can compute numerical approximations of differential operators with a desired degree of accuracy on particle-based stencils located in the physical domains of dependance.

The first-order ($O(\Delta t, \Delta x)$ upwinding discretization of the system (13-14) is obtained by the 1st order discretization of spatial derivatives based on the local polynomial fitting, and the 1st order discretization of temporal derivatives of the state (V, u or P) at the location of particle j,

$$\frac{state_j^{n+1} - state_j^n}{\Delta t}.$$

After the updates of states of each Lagrangian particle, particles are advanced by a mixture of the forward Euler scheme and backward Euler scheme:

$$\frac{x^{n+1} - x^n}{\Delta t} = \frac{1}{2}\left(u^n + u^{n+1}\right) \tag{16}$$

The first order scheme is stable, provided that the standard CFL condition is satisfied: $dt <= l/c$, where l is the smallest interparticle distance, but diffusive. To reduce the amount of numerical diffusion of the 1st order scheme and obtain a higher order approximation on space and time, we propose a *modified Beam-Warming* scheme for the Lagrangian particle system. For the same reason as in the original work on the Beam-Warming method [14], an additional term is added to equation (3):

$$\begin{aligned} U_t + A(U)U_x - \frac{\Delta t}{2}A^2(U)U_{xx} &= 0 \\ \Rightarrow U_t = -R\Lambda R^{-1}U_x + \frac{\Delta t}{2}R\Lambda^2 R^{-1}U_{xx} & \\ \Rightarrow R^{-1}U_t = -\Lambda R^{-1}U_x + \frac{\Delta t}{2}\Lambda^2 R^{-1}U_{xx}. & \end{aligned} \tag{17}$$

Equations (11) and (12) then become

$$
\begin{aligned}
-\frac{1}{2\sqrt{K}}u_t - \frac{1}{2K}P_t &= -V_0\sqrt{K}\left[-\frac{1}{2\sqrt{K}}u_{xl} - \frac{1}{2K}P_{xl}\right] \\
&+ \frac{\Delta t}{2}V_0^2 K\left[-\frac{1}{2\sqrt{K}}u_{xxl} - \frac{1}{2K}P_{xxl}\right], \qquad (18)\\
\frac{1}{2\sqrt{K}}u_t - \frac{1}{2K}P_t &= V_0\sqrt{K}\left[\frac{1}{2\sqrt{K}}u_{xr} - \frac{1}{2K}P_{xr}\right] \\
&+ \frac{\Delta t}{2}V_0^2 K\left[\frac{1}{2\sqrt{K}}u_{xxr} - \frac{1}{2K}P_{xxr}\right]. \qquad (19)
\end{aligned}
$$

Solving equations (10), (18) and (19) yields

$$
\begin{aligned}
V_t &= \frac{V_0}{2}\left(u_{xr} + u_{xl}\right) - \frac{V_0}{2\sqrt{K}}\left(P_{xr} - P_{xl}\right), \\
&+ \frac{\Delta t}{4}\left[V_0^2\sqrt{K}\left(u_{xxr} - u_{xxl}\right) - V_0^2\left(P_{xxr} + P_{xxl}\right)\right], \qquad (20)\\
u_t &= \frac{V_0\sqrt{K}}{2}\left(u_{xr} - u_{xl}\right) - \frac{V_0}{2}\left(P_{xr} + P_{xl}\right), \\
&+ \frac{\Delta t}{4}\left[V_0^2 K\left(u_{xxr} + u_{xxl}\right) - V_0^2\sqrt{K}\left(P_{xxr} - P_{xxl}\right)\right], \qquad (21)\\
P_t &= -\frac{V_0 K}{2}\left(u_{xr} + u_{xl}\right) + \frac{V_0\sqrt{K}}{2}\left(P_{xr} - P_{xl}\right), \\
&+ \frac{\Delta t}{4}\left[-V_0^2 K^{\frac{3}{2}}\left(u_{xxr} - u_{xxl}\right) + V_0^2 K\left(P_{xxr} + P_{xxl}\right)\right]. \qquad (22)
\end{aligned}
$$

By discretizing spatial derivatives using the second order local polynomial fitting, as described in Section 3.3, we obtaine numerical scheme that is second order in both time and space, $O(\Delta t^2, \Delta x^2, \Delta t \Delta x)$, and conditionally stable. The CFL condition is simlar to the one of the grid-based Beam-Warming scheme: in 1D, $dt <= 2l/max(c, u)$. Note that time steps can be twice larger compared to the 1st order scheme.

3.2. Time Integration and Directional Splitting

In this section, we focus on details of multidimensional schemes. We present explicit formulas for equations in the three-dimensional space. The system in the two-dimensional space is obtained by obvious reductions.

In the three-dimensional space, the conservative form of the Lagrangian formulation of the Euler equations is:

$$U_t^{'} + \left[F_1(U^{'})\right]_x + \left[F_2(U^{'})\right]_y + \left[F_3(U^{'})\right]_z = 0, \tag{23}$$

where

$$U^{'} = \left[\begin{array}{ccccc} V & u & v & w & E \end{array} \right]^T,$$

$$F_1(U^{'}) = V_0 \begin{pmatrix} -u \\ P \\ 0 \\ 0 \\ Pu \end{pmatrix}, \; F_2(U^{'}) = V_0 \begin{pmatrix} -v \\ 0 \\ P \\ 0 \\ Pv \end{pmatrix}, \; F_3(U^{'}) = V_0 \begin{pmatrix} -w \\ 0 \\ 0 \\ P \\ Pw \end{pmatrix}. \tag{24}$$

Assuming that the EOS is of the form $e = f\,(P, V)$ and using $U = [V \; u \; v \; w \; P]^T$ as the state vector, we can rewrite the equations in the following form

$$U_t + A_1 U_x + A_2 U_y + A_3 U_z = 0, \tag{25}$$

where

$$U = \begin{pmatrix} V \\ u \\ v \\ w \\ P \end{pmatrix}, \quad A_1 = V_0 \begin{pmatrix} 0 & -1 & 0 & 0 & 0 \\ 0 & 0 & 0 & 0 & 1 \\ 0 & 0 & 0 & 0 & 0 \\ 0 & 0 & 0 & 0 & 0 \\ 0 & K & 0 & 0 & 0 \end{pmatrix},$$

$$A_2 = V_0 \begin{pmatrix} 0 & 0 & -1 & 0 & 0 \\ 0 & 0 & 0 & 0 & 0 \\ 0 & 0 & 0 & 0 & 1 \\ 0 & 0 & 0 & 0 & 0 \\ 0 & 0 & K & 0 & 0 \end{pmatrix}, \quad A_3 = V_0 \begin{pmatrix} 0 & 0 & 0 & -1 & 0 \\ 0 & 0 & 0 & 0 & 0 \\ 0 & 0 & 0 & 0 & 0 \\ 0 & 0 & 0 & 0 & 1 \\ 0 & 0 & 0 & K & 0 \end{pmatrix}, \tag{26}$$

where K is defined in equation (5). We solve the system of hyperbolic PDEs (25 - 26) by using the directional splitting method by Strang [15]. Specifically, instead of solving equation (25), one solves separately the following three system of PDEs:

$$U_t + 3A_1 U_x = 0, \tag{27}$$

$$U_t + 3A_2 U_y = 0, \tag{28}$$

$$U_t + 3A_3 U_z = 0, \tag{29}$$

which is equivalent to solving

$$U_{1t} + 3AU_{1x} = 0, \tag{30}$$
$$U_{2t} + 3AU_{2y} = 0, \tag{31}$$
$$U_{3t} + 3AU_{3z} = 0, \tag{32}$$

where

$$U_1 = \begin{pmatrix} V \\ u \\ P \end{pmatrix}, U_2 = \begin{pmatrix} V \\ v \\ P \end{pmatrix}, U_3 = \begin{pmatrix} V \\ w \\ P \end{pmatrix}, A = V_0 \begin{pmatrix} 0 & -1 & 0 \\ 0 & 0 & 1 \\ 0 & K & 0 \end{pmatrix}. \tag{33}$$

Each of the three system of equations (30) - (32) is solved by the techniques introduced in section 3.1, and the solutions are combined in the following order

$$\begin{pmatrix} V \\ u \\ v \\ w \\ p \end{pmatrix}^{(0)} \xrightarrow{(30)} \begin{pmatrix} V \\ u \\ v \\ w \\ p \end{pmatrix}^{(\frac{\Delta t}{6})} \xrightarrow{(31)} \begin{pmatrix} V \\ u \\ v \\ w \\ p \end{pmatrix}^{(\frac{2\Delta t}{6})} \xrightarrow{(32)} \begin{pmatrix} V \\ u \\ v \\ w \\ p \end{pmatrix}^{(\frac{4\Delta t}{6})}$$
$$\xrightarrow{(31)} \begin{pmatrix} V \\ u \\ v \\ w \\ p \end{pmatrix}^{(\frac{5\Delta t}{6})} \xrightarrow{(30)} \begin{pmatrix} V \\ u \\ v \\ w \\ p \end{pmatrix}^{(\Delta t)} \tag{34}$$

where Δt denotes one discrete time step satisfying the CFL condition. The Strang splitting method maintains the second order of accuracy if the accuracy of each step is not lower than second, making it unnecessary for the 1st order numerical scheme. To implement the modified Beam-Warming scheme within the Strang splitting steps (30) - (32), we solve the following equations

$$U_{1t} + 3\left(AU_{1x} - \frac{\Delta t}{2}A^2U_{1xx}\right) = 0, \tag{35}$$
$$U_{2t} + 3\left(AU_{2y} - \frac{\Delta t}{2}A^2U_{2yy}\right) = 0, \tag{36}$$
$$U_{3t} + 3\left(AU_{3z} - \frac{\Delta t}{2}A^2U_{3zz}\right) = 0. \tag{37}$$

The solutions to equations (35) - (37) are then combined by equation (34) to obtain the complete second order solution to equation (25).

3.3. Local Polynomial Fitting

The local polynomial fitting on arbitrary sets of points has long been used to obtain approximation of functions and their derivatives. Details of the method and its accurracy is discussed in [16, 18, 19]. Generally, νth order derivative can be approximated with $(n-\nu+1)$th order of accuracy using nth order polynomial. For simplicity, a 2D example is discussed here. In the vicinity of a point 0, the function value in the location of a point i can be expressed by the Taylor series as

$$U_i = U_0 + h_i \left.\frac{\partial U}{\partial x}\right|_0 + k_i \left.\frac{\partial U}{\partial y}\right|_0 + \frac{1}{2}\left(h_i^2 \left.\frac{\partial^2 U}{\partial x^2}\right|_0 + k_i^2 \left.\frac{\partial^2 U}{\partial y^2}\right|_0 + 2h_i k_i \left.\frac{\partial^2 U}{\partial x \partial y}\right|_0 \right) + \ldots, \tag{38}$$

where U_i and U_0 are the corresponding function values in the location of points i and 0, $h_i = x_i - x_0$, $k_i = y_i - y_0$, and the derivatives are calculated in the location of the point 0. A polynomial can be used to approximate the original function and we employ a second order polynomial in this example:

$$\tilde{U} = U_0 + h_i\theta_1 + k_i\theta_2 + \frac{1}{2}h_i^2\theta_3 + \frac{1}{2}k_i^2\theta_4 + h_i k_i \theta_5. \tag{39}$$

Here the variables θ_1, θ_2, θ_3, θ_4 and θ_5 are the estimates for $\frac{\partial U}{\partial x}$, $\frac{\partial U}{\partial y}$, $\frac{\partial^2 U}{\partial x^2}$, $\frac{\partial^2 U}{\partial y^2}$, and $\frac{\partial^2 U}{\partial x \partial y}$, respectively. In order to compute values of these variables, we perform a local polynomial fitting using $m >= 5$ points in the vicinity of center point 0. The following linear system $Ax = b$

$$\begin{bmatrix} h_1 & k_1 & \frac{1}{2}h_1^2 & \frac{1}{2}k_1^2 & h_1k_1 \\ h_2 & k_2 & \frac{1}{2}h_2^2 & \frac{1}{2}k_2^2 & h_2k_2 \\ \vdots & \vdots & \vdots & \vdots & \vdots \\ h_n & k_n & \frac{1}{2}h_n^2 & \frac{1}{2}k_n^2 & h_nk_n \end{bmatrix} \begin{bmatrix} \theta_1 \\ \theta_2 \\ \theta_3 \\ \theta_4 \\ \theta_5 \end{bmatrix} = \begin{bmatrix} U_1 - U_0 \\ U_2 - U_0 \\ \vdots \\ U_n - U_0 \end{bmatrix}, \tag{40}$$

is usually overdetermined. As a proper selection of a neighborhood is important for accuracy and stability, neighbor search algorithms used in our upwind solvers are described in the next subsection.

An optimal solution to (40) is a solution x that minimizes the L_2 norm of the residual, i.e.,

$$min\|Ax - b\|_2, \tag{41}$$

and the QR decomposition with column pivoting is employed to obtain x. Suppose

$$A = Q \begin{bmatrix} R \\ 0 \end{bmatrix} P^T, m \geq n, \tag{42}$$

where Q is an orthonomal matrix, R is an upper triangle matrix, and P is a permutation matrix, chosen (in general) so that

$$|r_{11}| \geq |r_{22}| \geq \cdots \geq |r_{nn}|. \tag{43}$$

Moreover, for each k,

$$|r_{kk}| \geq \|R_{k:j,j}\|_2 \tag{44}$$

for $j = k+1, \cdots, n$. One can numerically determine an index k, such that the leading submatrix R_{11} in the first k rows and columns is well conditioned and R_{22} is negligible:

$$R = \begin{bmatrix} R_{11} & R_{12} \\ 0 & R_{22} \end{bmatrix} \simeq \begin{bmatrix} R_{11} & R_{12} \\ 0 & 0 \end{bmatrix} \tag{45}$$

Then k is the effective rank of A. Discussion about the numerical rank determination can be found in [20]. A simple way to determine numerical rank is to set a tolerance ϵ and find the first k such that

$$R_{kk} < \epsilon R_{11}. \tag{46}$$

If there is such k, then the effective numerical rank is $k-1$. The choice of ϵ is 10^{-3} in many of the test problems discussed in later sections. The solution for linear system (40) can be obtained as

$$x = P \begin{bmatrix} R_{11}^{-1} c_1 \\ 0 \end{bmatrix} \tag{47}$$

where c_1 is the first k elements of $c = Q^T b$. This can also be written as

$$x = A^+ b, \tag{48}$$

where

$$A^+ = P \begin{bmatrix} R_{11}^{-1} & 0 \\ 0 & 0 \end{bmatrix} Q^T \tag{49}$$

is the pseudoinverse of matrix A.

3.4. The neighbor Search Algorithm and Dynamic Stencil Selection

In a simulation involving N Lagrangian particles, a new *stencil* of neighbors - those particles used for solving equation (40) - is to be selected at the begining of each time step for all the N particles. As a result, it is critical that an efficient neighbor search algorithm is employed. The neighbor search method is described in the next subsection. While the neighbor search is to obtain a group of particles lying within some pre-specified distance away from the particle of interest, it is not necessary that all these neighbors are used in numerical stencils. The selection of stencil points from neighbors to ensure the accuracy and stability is discussed in Subsection 3.4.2.

3.4.1. Neighbor Search Algorithms

One of the main advantagees of the Lagrangian particle method compared to grid-based methods is its ability to simulate large and extremely non-uniform domains. By a non-uniform domain we mean a domain in which only a small fraction of the total volume occupied by matter, found typically in astrophysics and high energy density physics, and other applications dealing with dispersed fragments of matter. For these applications, we use 2^k-tree neighbor search algorithms [21]. The 2^k-tree is a tree data structure in a k-dimensional space in which each node has at most 2^k dependents. Quadtree and octree are the standard terms in 2D and 3D spaces, respectively. The tree construction can be performed with $O(N \log N)$ operation. In this process, the choice of the tree depth is essential and the optimal empirical number is four or five. After the construction step, the search of a tree for obtaining the neighborhood of a particle can be performed with $O(\log N)$ operation.

However the 2^k-tree method is not universally optimal for all types of problems. If the computational domain is almost uniformly filled with a weakly compressible matter in which inter-particle distances change insignificantly during the simulation allowing the use of the same neighbor search radius for all particles, the search of neighbors can be performed in constant time. In this case, we use the bucket search algorithm [9]. The entire computational domain is divided into square (cubic) cells of the side length equal to the search radius r. For each particle inside a cell, only the neighboring cells need to be considered in the search process. Clearly, the method is not optimal if the location of matter in the space is very sparse, and is not applicable if different search radii must be used for different particles. The 2^k-tree neighbor search algorithm is more universal and applicable to a wide range

of problems. In a forthcoming paper, we will describe an optimal parallel octree neighbor search algorithm for a 3D Lagrangian particle code.

3.4.2. Dynamic stencil selection

After the neighbor search step, each particle obtains a list of neighbors which lie within the range of a pre-specified search radius. To enforce upwinding, however, only one-sided information should be used when solving equation (40). For the calculation of one-sided derivatives, each particle will, in general, have four one-sided neighborhoods in two-dimensions, and six neighborhoods in three-dimensions.

Without loss of generality, the process of the dynamic stencil selection will be discussed using an example of computing u_{xr}. After gathering one-sided neighbors, two main issues must be resolved for accurate evaluation of spatial derivatives. The first one is related to the *shape* of the neighborhood. The list of one-sided neighbors is sorted by their distance from the center particle in ascending order. Suppose we obtain the following sorted list of neighbors of the particle 0 for computing u_{xr}:

$$\left\{p_{1u},\, p_{2u},\, p_{3l},\, p_{4u},\, p_{5u},\, p_{6u},\, p_{7l},\, p_{8u},\, p_{9l}\right\}.$$

Here the subscripts u and l indicate the upper and lower half-planes in the y-direction: $y_i >= y_0$ and $y_i < y_0$, respectively. If a simple distance-based algorithm picks up six neighbors, then the corresponding stencil is composed of

$$\left\{p_{1u},\, p_{2u},\, p_{3l},\, p_{4u},\, p_{5u},\, p_{6u}\right\},$$

thus producing a highly *unbalanced* stencil in terms of the *shape*. Therefore, besides sorting neighbors in ascending order of the distance from the center particle, the order is rearranged such that neighbors from the upper half and lower half occur interchangeably in the list

$$\left\{p_{1u},\, p_{3l},\, p_{2u},\, p_{7l},\, p_{4u},\, p_{9l},\, p_{5u},\, p_{6u},\, p_{8u}\right\}$$

The six-particle stencil now becomes:

$$\left\{p_{1u},\, p_{3l},\, p_{2u},\, p_{7l},\, p_{4u},\, p_{9d}\right\}$$

This approach yields more balanced-in-shape stencils, and typically results in more accurate spatial derivatives.

The second issue is the optimization of the *number* of neighbors for solving equation (40). In the case of second order local polynomial fitting, for example, five neighbors are required to solve equation (40). However, as equation (46) suggests, the effective rank of the matrix A in equation (40) may be less than five if

$$R_{kk} < \epsilon R_{11},\ k = 2, 3, 4, 5. \tag{50}$$

To avoid rank deficiency, a dynamic process for selecting neighbors into the stencil is designed. First, select the *tolerance* parameter ϵ as in equation (46). For the case of second order local polynomial fitting, one starts with five or six neighbors in the stencil. Based on this stencil, the QR decomposition with column pivoting is performed. Then determine the effective rank by equation (46). If the effective rank is no less than five, the stencil is complete. Otherwise, the next neighbor in the neighbor list is added to the stencil. The process continues until the effective rank is regained. For instance, in some cases one may need to use seven neighbors to gain an effective rank of five. Our algorithms uses much smaller number of neighbor particles compared to the modified versions of SPH such as Godunov-SPH, P-SPH, PHANTOM etc. that may require hundreds of particles [11].

In certain cases, the neighbor list may not contain sufficient number of particles needed by a stencil. In such a case, one may consider lowering the order of local polynomial fitting for this particle in the given direction. Lowering to first order local polynomial fitting requires only an effective rank of two for the two-dimensional case.

3.5. Limiters

The second order Lagrangian particle algorithm based on the modified Beam-Warming scheme is dispersive. To eliminate the resulting oscillations, a new type of limiter based on divided difference was developed and coupled with the numerical integration. The application of the algorithm with the limiter is demonstrated in section 4.

In the flux-limiter method [] TODO, the magnitude of the correction depends on the smoothness of data (represented by Φ), and can be written as

$$F(U; j) = F_L(U; j) + \Phi(U; j)[F_H(U; j) - F_L(U; j)] \tag{51}$$

In order to measure the smoothness of data, we can use the ratio of consecutive gradients:

$$\theta_j = \frac{U_j - U_{j-1}}{U_{j+1} - U_j} \tag{52}$$

Or we can use the average of the ratio of consecutive gradients from both directions:

$$\theta_j = \frac{1}{2}\left(\frac{U_j - U_{j-1}}{U_{j+1} - U_j} + \frac{U_{j+1} - U_j}{U_j - U_{j-1}}\right) \tag{53}$$

Equation (53) has the advantage that it is symmetric. If θ_j is near 1 the data is presumably smooth. If θ_j is far from 1 there may be discontinuity near data U_j. Let $\Phi(U; j) \equiv \phi_j$ to be a function of θ_j:

$$\phi_j = \phi(\theta_j) \tag{54}$$

Van Leer [**?**] proposed a smooth limiter function

$$\phi(\theta) = \frac{|\theta| + \theta}{1 + |\theta|} \tag{55}$$

We let $\phi(\theta) = 0$ for $\theta < 0$ or when θ is arbitrarily large. Nore that $\theta < 0$ in the case when $U_{j+1} - U_j$ and $U_j - U_{j-1}$ are in opposite signs in both equations (52) and (53)). θ is arbitrarily large when $U_{j+1} - U_j = 0$ in equation (52) and when $U_{j+1} - U_j = 0$ or $U_j - U_{j-1} = 0$ in equation (53).

Without loss of generality, we demonstrate the idea using the flux for volume. Remind that in the proposed Lagrangian particle method the volume flux is defined as (equation (**??**))

$$\begin{aligned} V_t = {} & \frac{V_0}{2}\left(u_{xr} + u_{xl}\right) - \frac{V_0}{2\sqrt{K}}\left(P_{xr} - P_{xl}\right) \\ & + \frac{\Delta t}{4}\left[V_0^2\sqrt{K}\left(u_{xxr} - u_{xxl}\right) - V_0^2\left(P_{xxr} + P_{xxl}\right)\right] \end{aligned} \tag{56}$$

Let the lower order flux (first order flux) of volume be defined as

$$F_L(V) = \frac{V_0}{2}\left(u_{xr(1)} + u_{xl(1)}\right) - \frac{V_0}{2\sqrt{K}}\left(P_{xr(1)} - P_{xl(1)}\right) \tag{57}$$

where the subscript (1) denotes the spatial derivatives obtained by first order polynomial fitting. Then define the higher order flux (second order flux) of

volume be defined as

$$F_H(V) = \frac{V_0}{2}\left(u_{xr(2)} + u_{xl(2)}\right) - \frac{V_0}{2\sqrt{K}}\left(P_{xr(2)} - P_{xl(2)}\right) + \frac{\Delta t}{4}\left[V_0^2\sqrt{K}\left(u_{xxr(2)} - u_{xxl(2)}\right) - V_0^2\left(P_{xxr(2)} + P_{xxl(2)}\right)\right] \tag{58}$$

where the subscript (2) denotes the spatial derivatives obtained by second order polynomial fitting.

In order to make the measure of the smoothness of data (θ) generalizable to higher dimensions and applicable to the Lagrangian particle mehtod, we propose using the one-sided spatial derivatives calculated by methods introduced in section 3.3. Depneding on the type of data we have, θ of a particle j is calculated as:

$$\theta_j(u) = \frac{u_{xl(1)}}{u_{xr(1)}} \tag{59}$$

$$\theta_j(P) = \frac{P_{xl(1)}}{P_{xr(1)}} \tag{60}$$

where u is the velocity in the x, y, or z-direction and P is the pressure. Alternatively, we can also use

$$\theta_j(u) = \frac{1}{2}\left(\frac{u_{xl(1)}}{u_{xr(1)}} + \frac{u_{xr(1)}}{u_{xl(1)}}\right) \tag{61}$$

$$\theta_j(P) = \frac{1}{2}\left(\frac{P_{xl(1)}}{P_{xr(1)}} + \frac{P_{xr(1)}}{P_{xl(1)}}\right) \tag{62}$$

Note that equations (61) and (62) are better over (59) and (60) since they are symmetric. We choose

$$\theta_j = \min(\theta_j(u), \theta_j(P)) \tag{63}$$

and calculate ϕ_j by (55). Note that we set $\phi_j = 0$ when $\theta_j < 0$ or θ_j is arbitrarily large. Substituting the calculated ϕ_j, the lower and higher flux in (57) and (58) into (51), we obtain the volume flux of particle j as:

$$F_j(V) = F_L(V; j) + \phi_j[F_H(V; j) - F_L(V; j)] \tag{64}$$

Then time integration gives the volume at next time step as:

$$V^{n+1} = V^n + \Delta t F_j(V) \tag{65}$$

Similarly to [22], we use the divided differences to detect the region that contains discontinuities. However, while the method of divided differences is used in [22] for choosing one of different stencils, it is employed in our work for switching between high order and low order discretization schemes.

The proposed limiter works as a switch between higher and lower order schemes to avoid the oscillatory behavior.

3.6. Modelling of Free Surfaces using Ghost Particles

An important feature of the Lagrangian particle method is its ability to robustly handle free surface flows with geometrically complex interfaces. The method is also generalizable to multiphase problems. Here by free surface flows we mean flows of fluid or gas in vacuum, and by multiphase problem we mean the interface dynamics between two immiscible fluids or gases. In this section, we describe an algorithm for physically consistent solutions at free fluid or gas interfaces.

The fluid / vacuum interface is modeled in our method by using *ghost* particles in the vacuum region. A geometric algorithm places patches of ghost particles outside the fluid boundary, ensures their proper distance to the interface, and eliminates those particles that were placed too closely or inside the fluid. Then the ghost particles are assigned physics states. The only functionality of ghost particles is to serve as neighbors of fluid particles when calculating spatial derivatives. Hence, only two states are relevant: pressure and velocity. As ghost particles represent vacuum, their pressure state is assigned to zero. A weighted 0th order local polynomial fitting is used to assign velocity states to ghost particles. This involves computing the weighted average of velocities of the fluid particles that are in a neighborhood of the ghost particle. Let's assume that the weighting function of the particle 0 in a three-dimensional space is $w(h_j, k_j, g_j)$, where $h_j = x_j - x_0$, $k_j = y_j - y_0$, $g_j = z_j - z_0$, and j is the index of neighbor particles. The velocity u_0 of particle 0 satisfies

$$\min_{u_0} \sum_{j=1}^{N} \left[(u_0 - u_j) w(h_j, k_j, g_j) \right]^2 , \tag{66}$$

which leads to the solution

$$u_0 = \frac{\sum_{j=1}^{N} u_j w_j^2}{\sum_{j=1}^{N} w_j^2} \tag{67}$$

This simple algorithm adequately handles the fluid / vacuum interface, but a Riemann solver-based algorithm will be used for interfaces in multiphase problems.

4. Numerical Results

In this section, we present results of one- and two-dimensional simulation that serve as verification tests for the Lagrangian particle method, including the free surface algorithm.

4.1. 1D Gaussian Pressure Wave Propagation with Periodic Boundaries

We study the propagation of a pressure wave in gas with the constant initial density $\rho = 0.01$ and the initial Gaussian pressure distribution

$$p = 5 + 2e^{-100x^2} \tag{68}$$

in the domain $-1.5 \leq x \leq 1.5$ with periodic boundaries on both ends. The polytropic gas EOS is used with $\gamma = 5/3$. The goal of the simulation is to demonstrate the accuracy of the proposed algorithm in resolving nonlinear waves with the formation of shocks. The benchmark data is obtained using a highly refined, grid-based MUSCL scheme. The results, shown in Figure 1, are labeled as *1st* for the first order local polynomial fitting, *B.W.* for the Beam-Warming scheme with second order local polynomial fitting, and *B.W. lim.* for the Beam-Warming scheme with the second order local polynomial fitting with limiter, respectively. As expected, first order scheme is diffusive, while the Beam-Warming scheme is dispersive near discontinuities. However, results demonstrates that the proposed limiter method effectively reduces dispersions near sharp edges, resulting in maintaining globally the second order of convergence.

We have also verified that the Lagrangian particle methods accurately resolves waves in stiff materials. We use the same initial pressure as before, but replace the polytropic EOS with the stiffened polytropic EOS

$$E = \frac{(P + \gamma P_\infty)\, V}{\gamma - 1} \tag{69}$$

with $\gamma = 6$ and $P_\infty = 7000$. The convergence results can be found in Tables 1 and 2. In both cases, the second order convergence is obtained.

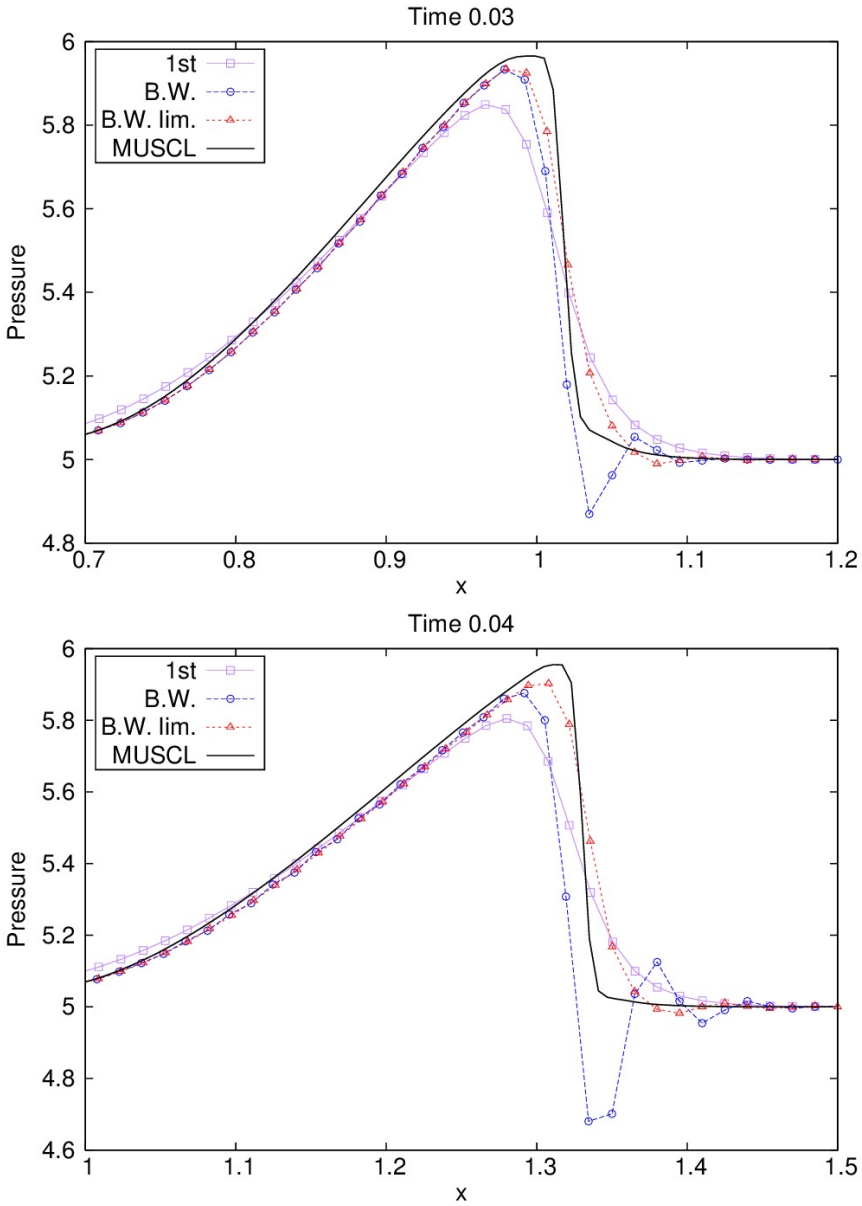

Figure 1: Gaussian pressure wave propagation with periodic boundaries at time 0.03 (top) and 0.04 (bottom). Coarse-resolution simulations results were used to illustrate the behavior qualitatively.

Number of particles	Relative $L2$-norm error	Rate of Convergence
240	0.051	NA
480	0.018	2.88
960	0.0049	3.60
1920	0.0012	4.02
3840	0.00029	4.23
7680	0.000068	4.24

Table 1: Convergence for the polytropic gas EOS case with $\gamma = \frac{5}{3}$ and initial density $\rho_0 = \frac{1}{V_0} = 0.01$

Number of particles	Relative $L2$-norm error	Rate of convergence
240	0.069	NA
480	0.021	3.23
960	0.0056	3.84
1920	0.0014	3.97
3840	0.00035	4.0
7680	0.000093	3.8

Table 2: Convergence for the stiffened polytropic gas EOS case with $\gamma = 6$, $P_\infty = 7000$, and initial density $\rho_0 = \frac{1}{V_0} = 1$

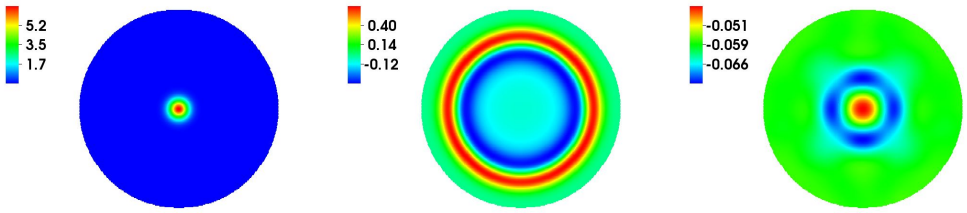

Figure 2: 2D Gaussian pressure wave propagation in disk with free surface. Pressure distribution (bar) at initial time (left), 10 (middle), and 60 (right).

4.2. 2D Gaussian Pressure Wave Propagation with Free Surface

To test the proposed algorithm for two-dimensional problems involving free surfaces, a circular disk of particles with stiffened polytropic gas EOS (with $\gamma = 6$, $P_\infty = 7000$, and $\rho = 1$) and a Gaussian pressure profile was initialized. The results are presented in two dimensions in Figure 2. Note that the latest-time plot in Figure 2 represents the state when the pressure waves have been reflected from the oscillatory free surface for more than ten times. To verify the accuracy, the analogous one-dimensional problem with cylindrical coordinates under the Eulerian formulation was solved using a refined MUSCL scheme with the method of front tracking for the free surface implemented in the FronTier code [6]. The location and shape of the pressure wave and the interface as well as the oscillatory motion of the free surface are in good agreement with the FronTier simulation. The verification test and the fact that the pressure wave maintains good symmetry after many reflections from the free surface demonstrate that the method for modeling vacuum introduced in section 3.6 works well with the proposed algorithm.

4.3. 2D Shock Tube Problem

4.4. Gresho Vortex

The Gresho problem is a steady-state rotating vortex roblem that has an exact analytic solution in the case of Euler equations [23]. Gresho vortex is a, inviscid gas vortex with such a radial distribution of the angular velocity u_ϕ and pressure, that the centripital force is compensated by the gradient of

pressure:

$$(u_\phi(r), p(r)) = \begin{cases} \left(5r, 5 + \frac{25}{2}r^2\right), & 0 \le r \le 0.2, \\ \left(2 - 5r, 9 - 4\ln 0.2 + \frac{25}{2}r^2 - 20r + 4\ln r\right), & 0.3 \le r \le 0.4, \\ \left(0, 3 + 4\ln 2\right), & 0.4 \le r. \end{cases} \tag{70}$$

This problem, known to be notoriously difficult for SPH, tests the accuracy of numerical scheme and its ability to preserve the symetry and angular momentum. The empirical is order of accuracy of second-order grid-based schemes for this problem, reported in literature, is approximately 1.4. Figure 3 shows the analytic solution and numerical simulation results of the vortex after one full rotation obtained with the Lagrangian particle method. The convergence is of second order at the initial stages of rotation, and it degrades to the first order in the later stages of rotation due to particle redistribution. For comparison, in Figure 4 we show simulations performed using grid-based schemes at the same numeircal resolution.

4.5. 2D Collision Between Two Circular Disks

In previous test problems, particles are initialized using regular distributions, such as the hexagonal packing, and slightly move with the flow. Nevertheless, the magnitude of the particle movement is quite restricted in previous tests, usually less than five percent of the initial inter-particle-spacing. In this section, a geometrically complex two-dimensional problem with large particle movement and object shape distortion is presented.

The setup of the problem is as follows. Two fluid disks have initially uniform density $\rho = 1$ and zero pressure, and material properties described by the stiffened polytropic EOS with $\gamma = 6$ and $P_\infty = 7000$. The two disks move toward each other with the relative longitudinal velocity of 20, but along lines that do not connect their centers. The time sequence shows the distortion of disks after the collision. While no benchmark data exists for such a problem, we believe that the results are reasonable from physics point of view as they agree with theoretical estimates of achievable pressure peaks. They demonstrate the ability of the proposed method to handle geometrically complex interfaces.

4.6. Gas expansion into Vacuum

5. Conclusions and Future Work

A Lagrangian particle method has been proposed for the simulation of Euler equations describing compressible inviscid fluids or gases. By repre-

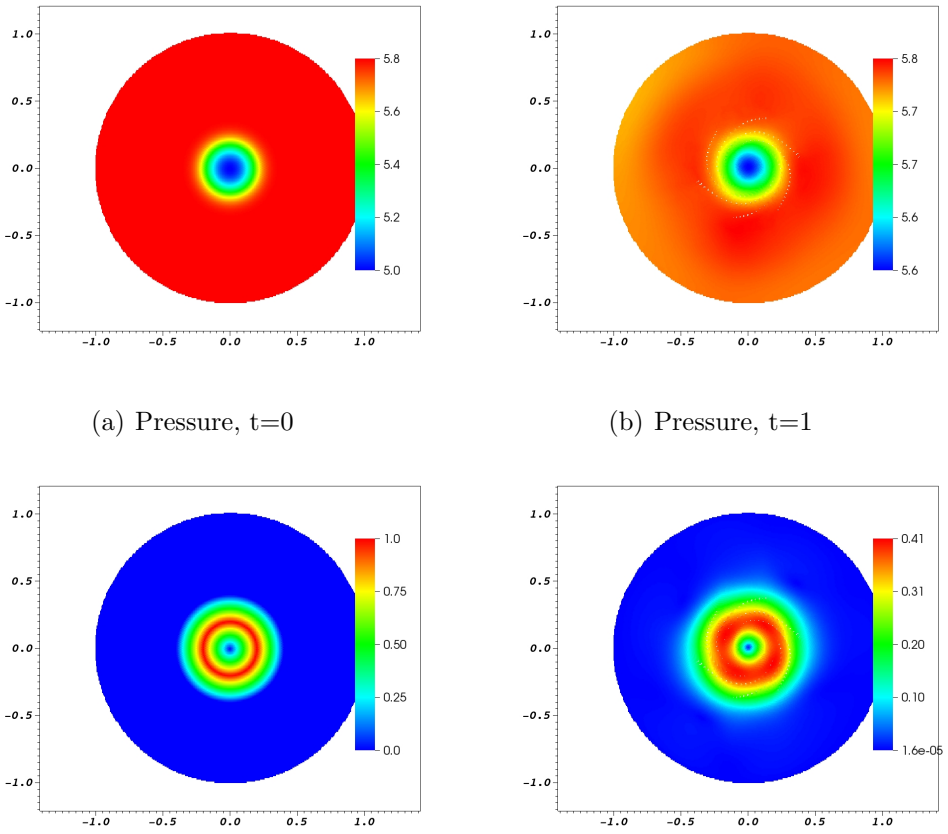

(a) Pressure, t=0

(b) Pressure, t=1

(c) Velocity, t=0

(d) Velocity, t=1

Figure 3: Exact solution (left column) and LP simulation (right column) of the Gresho vortex. Top row images depict pressure and bottom row images depict density.

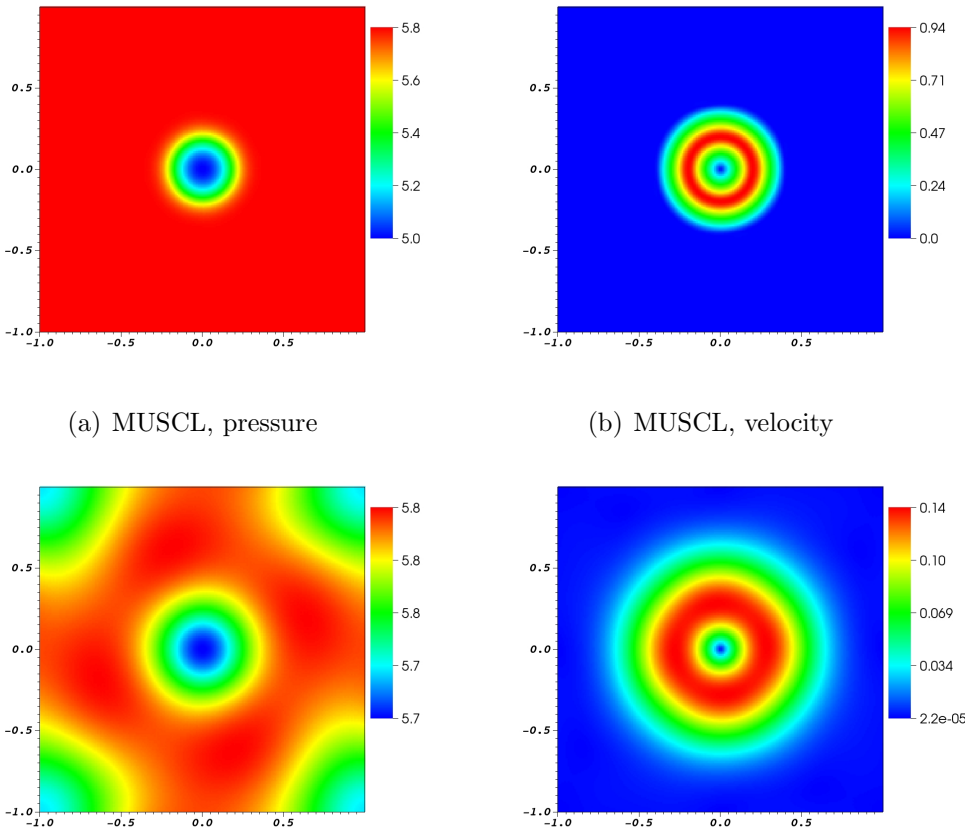

(a) MUSCL, pressure

(b) MUSCL, velocity

(c) LF, pressure

(d) LF, velocity

Figure 4: Simulations of the Gresho vortex using MUSC scheme (top row images) and Lax Friedrichs scheme (bottom row images). Left column of images depict pressure and right column of images depict density.

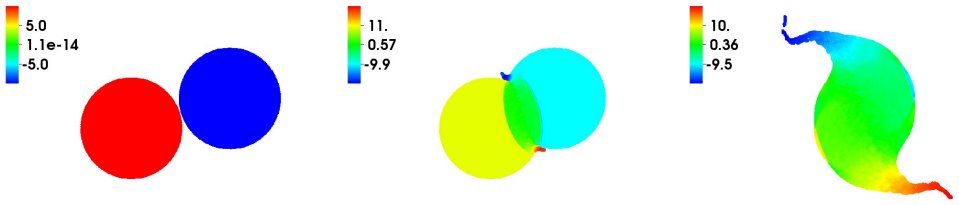

Figure 5: 2D simulation of collision of two disks. Velocity distribution (10 m/s) at initial time (left), 21 (middle), and 54 (right).

senting Lagrangian fluid cells with particles, similarly to smoothed particle hydrodynamics, the method eliminates the mesh distortion problem of the original Lagrangian method and is suitable for the simulation of complex free surface flows. The main contributions of our method, which is different from SPH in all other aspects, are (a) significant improvement of approximation of differential operators based on polynomial fits and the corresponding weighted least squares problems and convergence of prescribed order, (b) an upwinding second-order particle-based algorithm with limiter, providing accuracy and long term stability, (c) elimination of the dependence on artificial parameters such as the smoothening length in SPH, causing difficulties especially in the case of large density changes, and (d) accurate resolution of states at free interfaces. Numerical verification tests demonstrate the second convergence order of the method and its ability to resolve complex free surface flows.

The Lagrangian particle method has numerous advantages compared to grid-based methods for the simulation of complex systems. It eliminates the need for complex and costly algorithms for the generation and adaptation of meshes, provides continuos adaptivity to density changes, and is suitable for extremely non-uniform domains typical for astrophysics or high energy density applications. The algorithmic complexity of key particle methods insignificantly increases with the increase of spatial dimensions, making a 3D code similar to a 1D code. In addition, particle algorithms are independent of the geometric complexity of domains. In contrast, there is a huge increase in algorithmic complexity of a 3D mesh generation and dynamic adaptation compared to 1D as well as the increase associated with the geometric complexity of domains.

The future development of the space-time discretization methods will explore new high resolution WENO-type solvers based on irregularly placed particle nodes and symplectic integrators. Our Lagrangian particle method is also generalizable to coupled multiphysics systems, including the dynamics of plasmas, incompressible fluids, and fracture of solids.

Acknowledgement. This research has been partially supported by the DOE Muon Accelerator Program. This manuscript has been authored in part by Brookhaven Science Associates, LLC, under Contract No. de-sc0012704 with the US Department of Energy. The United States Government retains, and the publisher, by accepting the article for publication, acknowledges, a world-wide license to publish or reproduce the published form of this manuscript, or allow others to do so, for the United States Government purpose.

References

[1] R.D. Richtmyer, K.W. Morton, *Finite diference methods for initial value problems*, Interscience, New York - London - Sydney, 1967.

[2] H. Lamb, *Hydrodynamics*, Cambridge Univ. Press,

[3] Hirt, C.W., Nichols, B.D. (1981), "Volume of fluid (VOF) method for the dynamics of free boundaries", J. Comput. Phys., 39 (1): 201225

[4] S. Osher, R. Fedkiw, Level Set Methods and Dynamic Implicit Surfaces, 2002, Springer-Verlag.

[5] C.W. Hirt, A.A. Amsden, J.L. Cook, An arbitrary Lagrangian-Eulerian computing method for a;; flow speeds, J. Comput. Phys, 135 (1997), 203-216.

[6] B. Fix, J. Glimm, X. Li, Y. Li, X. Liu, R. Samulyak, and Z. Xu. A TSTT integrated Frontier Code and its applications in computational fluid physics. *Journal of Physics: Conf. Series*, 16:471–475, 2005.

[7] J. J. Monaghan, Smoothed Particle Hydrodynamics, In: Annual review of astronomy and astrophysics. Vol. 30, p. 543-574. 1992.

[8] J. J. Monaghan, Smoothed particle hydrodynamics, Rep. Prog. Phys., 68 (2005), 1703 – 1759.

[9] J. J. Monaghan, J. C. Lattanzio. A Refined Particle Method for Astrophysical Problems, Astronomy and Astrophysics, vol. 149, no. 1, Aug. 1985, p. 135-143.

[10] G. A. Dilts, Moving-least-squares particle hydrodynamics I. Consistency and stability. Int. J. Num. Methods in Engineering, 44 (1999), 1115 – 1155.

[11] P. F. Hopkins, GIZMO: a new class of accurate, mesh-free hydrodynamic simulation methods, Mon. Not, R. Astron. Soc., 2014.

[12] F. Urena, J. J. Benito, L. Gavete, Application of the generalized finite difference method to solve the advection-diffusion equation, J. Comp. Appl. Math., 235 (2011), 1849 - 1855.

[13] D. Price, Smoothed particle hydrodynamics and magnetohydrodynamics, arxiv.org:1012.1885v1

[14] J.L. Steger, R.F. Warming, Flux vector splitting of the inviscid gas dynamic equations with application to finite-difference methods, J. Comput. Phys., 40 (1981), 263 - 293.

[15] G. Strang, On the construction and comparison of difference schemes, SIAM J. Numerical Analysis, 5 (1968), 506-517.

[16] J.J. Benito, F. Urena, L. Gavete, Influence of several factors in the generalized finite difference method, Applied Math. Modeling, 25 (2001), 1039-1053.

[17] R. Courant, K.O. Friedrichs, *Supersonic flow and shock waves*, Springer, 1999.

[18] Jianqing Fan, Theo Gasser, Irene Gijbels, Michael Brockmann, and Joachim Engel. Local polynomial fitting: A standard for nonparametric regression, 1993.

[19] X. Jiao and H. Zha. Consistent computation of first- and second-order differential quantities for surface meshes. *ACM Solid and Physical Modeling Symposium*, 2008. (Available at arxiv.org/abs/0803.2331)

[20] G. GOLUB and C. F. VAN LOAN. *Matrix Computations*. Johns Hopkins University Press, Baltimore, MD, 1996.

[21] H. Samet, The design and analysis of spatial data structures, Adison-Wesley Publishing Company, 1990.

[22] Chi-Wang Shu, Essentially Non-Oscillatory and Weighted Essentially Non-Oscillatory Schemes for Hyperbolic Conservation Laws, NASA/CR-97-206253, ICASE Report No. 97-65, Nov. 1997

[23] R. Liska, B. Wendroff, Comparison of several difference schemes on 1D and 2D test problems for the Euler equations, SIAM J. Sci. Comput., 25 (2003), 9951017.